JTTEE5 19:448–458
DOI: 10.1007/s11666-009-9449-4
1059-9630/$19.00 © ASM International

A Novel Single Cathode Plasma Column Design for Process Stability and Long Component Life

P.S. Mohanty, A. George, L. Pollard, and D. Snyder

(Submitted April 24, 2009; in revised form August 29, 2009)

This paper investigates a novel single cathode plasma column design consisting of a patented arc constrictor and its impact on process stability, versatility, and component life. The design aims to minimize the re-strike of arc, increase the arc length enabling high voltage and low amp operation as well as the use of ternary gas combination to increase the enthalpy. The arc unsteadiness and dynamic behavior are investigated through the fluctuations of electrical signals. Further, the particle velocity and temperature have been characterized by commercial diagnostics systems. The takeover/steady mode appears to be the typical operational mode of the plasma jet in this design. Low amplitude and high frequency fluctuations resulted in steady particle characteristics. Further, the design allowed the gun to operate at very high plasma velocities reaching the characteristics of an HVOF jet. The significance of the design is demonstrated through operational flexibility and stability.

Keywords arc fluctuation, diagnostics, plasma column design

1. Introduction

Despite being a well-established industrial technology, the reliability and reproducibility of DC plasma spray process are limited, which mainly emerge from the inherent instabilities of the arc and the associated phenomena. Although much of the earlier developments in torch design to improve the torch stability and electrode wear reduction relied on empirical procedures, recent studies have been devoted to a basic understanding of the arc physics and the plasma jet dynamics (Ref 1-15). In most single cathode/anode DC plasma torches, the arc column is roughly parallel to the anode surface, and a cold gas boundary (CBL) layer electrically insulates the arc column from the anode. It is well understood that the arc strikes from the tip region of the cathode to some point on the anode wall where it attaches in the form of a high-temperature, low-density gas column cutting through the CBL that covers the anode wall (Ref 15). While the arc attempts to attach to the anode surface, the drag force exerted by the flow in the boundary layer and the Lorentz forces try to pull it away. The combined action of the drag and Lorentz forces make the anode arc attachment to exhibit an axial and rotational movement on the anode surface.

The thickness of the CBL controls the arc behavior and depends on the plasma torch working parameters, namely, the inner column design (cathode, anode, and exit nozzle), the arc current intensity, and the plasma gas flow dynamics. The symmetry of the anode design favors the rotational movement of the arc. This rotational movement results in a statistically average enthalpy input to the gas. On the other hand, the axial displacement of the arc root brings a variation in the length of the arc column and, therefore, in the enthalpy input to the gas. These variations in the length and width of the arc column give rise to temporal variations in gas temperature and velocity of the jet. In most torch designs, the resulting variation in gas temperature and velocity has a period that is similar in magnitude to the traverse time of the powder particles in the plasma jet (0.1-1 ms) leading to a non-uniform heating and transport of the injected powder and, consequently, affect the coating qualities. The electrode life, thermal efficiency, and performance of the plasma devices are directly or indirectly attributed to the nature of arc fluctuations (Ref 11, 15, 16).

Concurrent with academic research focused on a better understanding of the fundamental mechanisms and the process parameters involved in the plasma source, studies have also focused on gun design and development for stable arc and in turn reliable operation. Various designs have been proposed, namely, double anode design (Ref 17), cascade design (Ref 18, 19), and triplex design

This article is an invited paper selected from presentations at the 2009 International Thermal Spray Conference and has been expanded from the original presentation. It is simultaneously published in *Expanding Thermal Spray Performance to New Markets and Applications: Proceedings of the 2009 International Thermal Spray Conference*, Las Vegas, Nevada, USA, May 4-7, 2009, Basil R. Marple, Margaret M. Hyland, Yuk-Chiu Lau, Chang-Jiu Li, Rogerio S. Lima, and Ghislain Montavon, Ed., ASM International, Materials Park, OH, 2009.

P.S. Mohanty and **A. George**, Additive Manufacturing Process Laboratory, University of Michigan, Dearborn, MI; and **L. Pollard** and **D. Snyder**, Progressive Technology Inc., Grand Rapids, MI. Contact e-mail: pmohanty@umich.edu.

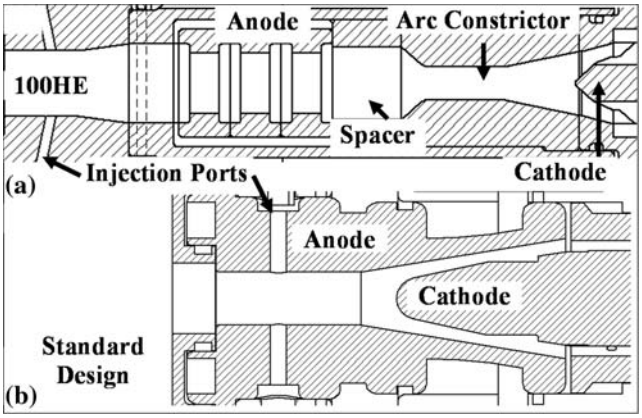

Fig. 1 (a) 100HE plasma column design and (b) typical plasma column design used in most single cathode systems

(Ref 20) etc., to control arc instabilities and the residence time of the arc at a given location to limit the heat load on the anode wall and, thus, its erosion. In this paper, a novel plasma column design with patented (Ref 21) single cathode/anode configuration is investigated. The goals of this design configuration are a weakly fluctuating long-arc, high-voltage-low-current operation and, in turn, reliable performance and long component life. The configuration of this single cathode plasma torch is shown in Fig. 1. Compared with the conventional plasma torch designs, here, the anode is separated from the cathode tip by an electrically insulated arc constrictor leading to a long arc (~70 mm) (Ref 22, 23). The anode consists of three internal tungsten rings within a copper block. The arc is initiated by a combination of the arc starter and an impulse signal that initiates the arc into the arc constrictor. The gas flow through the constrictor pushes the arc to the anode. Based on this design, a commercial torch named as 100HE is marketed by Progressive Technology Inc., Grand Rapids, MI. This gun maintains a much higher arc voltage and a relatively low arc current as well as uses a ternary gas. Typical operating ranges are 200-275 V, 375-600 A, and 25-100 kW. Based on the chiller data, the general range of thermal efficiencies of the torch is 38% at 70 kW and 57% at 100 kW. The influence of gas flow rate, gas mixture type, and arc current intensity on the arc fluctuations and dynamic behavior of the plasma jet is investigated by means of standard tools, such as the transient voltage/current analysis, FFT and particle temperature/velocity measurements. Further, the influence of the arc behavior on the long-term performance of the components, process stability, and efficiency are discussed.

2. Experimental

The arc behavior in the plasma jet has been the subject of numerous experimental studies (Ref 1, 2, 9-14). The fast Fourier transform (FFT) method has been widely used for the analysis of electrical, optical, and acoustical signals to reflect local or global manifestations of arc fluctuations. Dorier et al. (Ref 10) have studied the arc root behavior of plasma gun by simultaneous measurements of the time-series of the arc voltage and images from the nozzle interior. Hlina et al. (Ref 1) have analyzed the oscillation phenomena in a jet based on evaluations of CCD (charge-couple device) camera records of plasma radiation. Duan and Heberlein (Ref 2) have studied the arc fluctuations with various plasma torch configurations. Bisson et al. (Ref 11) have conducted simultaneous measurement of the arc voltage and its influence on particle temperature and velocity. Janisson et al. (Ref 13) have studied the gas mixture effect on the arc fluctuations. Elegant numerical models (Ref 4-8, 15) of the phenomenon have also been developed.

Measurement techniques employed in this investigation involved voltage and current traces as well as particle temperature and velocity. The data acquisition setup consisted of a PC (personal computer), a NI SCXI 1000 4-slot chassis, SCXI 1600 USB Data Acquisition (DAQ) Module, two SCXI 1120 devices with two high-voltage attenuator blocks of SCXI 1327 (National Instruments, Austin, TX). The device was configured for an input of 0-10 V and the gun anode and cathode terminals were connected to the DAQ device through a voltage transducer, CV 3-500 (300 kHz bandwidth) which converts the gun voltage (~0 to 500 V) to a voltage of 0-10 V. Care was taken to ensure that the sampling rate of the setup was capable of measurements up to 100 kHz frequency, and the sampling rate was set at 200 kS/s to satisfy the Nyquist criterion. The data were stored in the PC for offline analysis in LabView (National Instruments, Austin, TX). Voltage fluctuations were sampled at the plasma torch to eliminate any resistive effects of the power cable. The current was measured using a Hall Effect transducer (HAL 400S, 50 kHz bandwidth, LEM, Milwaukee, WI) in the power supply. Particle temperature and velocity measurements were done by DPV 2000 (Tecnar Inc., Canada) as well as SprayWatch 2i (Oseir Ltd., Finland) diagnostics systems.

The 100HE gun uses Ar as the primary gas, N_2 as the secondary gas, and H_2 or He as the ternary gas. The use of diatomic and heavy secondary gas (N_2) gives the ability to achieve high enthalpy input and velocity simultaneously. Ternary gas of either H_2 or He gives the ability to adjust the plasma characteristics further. In fact, the use of these gases enables the gun to offer a process window bridging the gap between traditional plasma gun and HVOF. The voltage, current, particle temperature, and velocity measurements were taken for various operating conditions as described in Table 1. Two flow conditions, 300 and 570 scfh, were investigated, hereafter referred as low-flow and high-flow, respectively. The gas ratio, Ar/N_2/ternary gas (H_2 or He), was varied while keeping the total flow constant within each flow conditions. The gas ratios denoted as 1, 2, and 3 in Table 1 were adjusted as follows. For ratio 1, the volume of secondary gas was almost twice of the ternary gas; for ratio 2, the volume of secondary and ternary gases was similar; and for ratio 3, the volume of secondary gas was almost half of the ternary gas. For each ratio, the volume of Ar was slightly adjusted to bring the total flow to a fixed value, i.e. 300 or 570 scfh. Three

Table 1 Experimental matrix

Series	Gas mixture, scfh: Ratio	Ar	N_2	H_2	He	Total flow, scfh	Amp	kW
100	1	189	75	36		300	400	70
101	2	195	54	51		300	400	71
102	3	201	33	66		300	400	72
103	1	360	142	68		570	400	96
104	2	370	102	97		570	400	98
105	3	382	62	125		570	400	98
200	1	189	75		36	300	400	42
201	2	195	54		51	300	400	47
202	3	201	33		66	300	400	50
203	1	360	142		68	570	400	61
204	2	370	102		97	570	400	67
205	3	382	62		125	570	400	72
300	1	189	75	36		300	300	55
301	2	195	54	51		300	300	55
302	3	201	33	66		300	300	55
303	1	360	142	68		570	300	73
304	2	370	102	97		570	300	73
305	3	382	62	125		570	300	74
400	1	189	75		36	300	300	33
401	2	195	54		51	300	300	36
402	3	201	33		66	300	300	38
403	1	360	142		68	570	300	48
404	2	370	102		97	570	300	51
405	3	382	62		125	570	300	55
500	1	189	75	36		300	200	38
501	2	195	54	51		300	200	38
502	3	201	33	66		300	200	37
503	1	360	142	68		570	200	49
504	2	370	102	97		570	200	49
505	3	382	62	125		570	200	49
600	1	189	75		36	300	200	22
601	2	195	54		51	300	200	25
602	3	201	33		66	300	200	27
603	1	360	142		68	570	200	33
604	2	370	102		97	570	200	35
605	3	382	62		125	570	200	38

current levels, 200, 300, and 400 A were considered in the study. Series 100, 300, and 500 experiments used hydrogen as the ternary gas while series 200, 400, and 600 used helium as the ternary gas. Both YSZ (yttria-stabilized zirconia, 20-106 μm, HC Starck, West Chester, OH) and 316 stainless powders (22-53 μm, Carpenter, Wyomissing, PA) were used for particle data.

3. Results and Discussion

The data were analyzed in the time domain as well as in the spectral domain by means of FFT computation. The FFT was taken by subtracting the mean from the data and also by low pass filtering the data so that the frequency components, characteristic of the gun operation can be extracted. Some useful information such as average voltage, $\bar{u}$, and the standard deviation, u_{sd}, was obtained from the time domain data. The calculations for $\bar{u}$ and u_{sd} are defined as follows:

$$\bar{u} = \frac{1}{N}\sum_{i=1}^{N} u_i \qquad \text{(Eq 1)}$$

$$u_{sd} = \sqrt{\frac{1}{N-1}\sum_{i=1}^{N}(u_i - \bar{u})^2} \qquad \text{(Eq 2)}$$

Different arc fluctuation modes have been defined in relation to the thickness of the cold boundary layer (Ref 2). Accordingly, certain figures of merit, which give an insight into the gun operation modes, were established. These include the amp factor (A) and shape factors (Sh). The shape factor Sh by definition is:

$$Sh = \frac{t_{up}}{t_{down}} = \frac{\text{number of instances where } u_{i+1} > u_i}{\text{number of instances where } u_{i+1} < u_i} \qquad \text{(Eq 3)}$$

where t_{up} and t_{down} denote the time duration of the up-rising slope and the downward slope, respectively. The underlying theory to this ratio is that in the restrike mode the voltage ramps up relatively slowly followed by a steep decline. During takeover mode, these times are relatively equal. This leads to a fundamental characteristic that the restrike mode has a high Sh factor, and the ideal takeover mode has a Sh value of 1. While the steady mode has a flat voltage trace resulting in a low $\bar{u}$ and u_{sd}. The steady mode has been linked to accelerated anode wear. An amp factor A was also introduced by Ref 2, but modified by Vysohlid (Ref 24) as a better method for measuring an irregular signal. The amp factor was calculated using the average voltage $\bar{u}$, standard deviation u_{sd}, and defined as follows:

$$A = \frac{u_{sd}}{\bar{u}} \times 100\% \qquad \text{(Eq 4)}$$

It has been previously established (Ref 2) that a perfect restrike mode exists when $A \geq 10$, and $Sh \geq 5$. A prefect takeover mode exists when $A \geq 10$ and $Sh < 1.1$. The steady mode was defined as $A < 2$, while a takeover-steady mixed mode was $2 < A < 10$, and the restrike-takeover mixed mode was $A \geq 10$ and $Sh < 5$.

For all the cases investigated here (Table 1), the condition of $2 < A < 10$ was observed indicating that the gun ran in a takeover-steady mixed mode; however, the shape factor was observed in the range $1.1 < Sh < 5$. Sample voltage and current traces for the gun, operating at ~71 kW for two different ternary gases (He and H_2), are presented in Fig. 2. As expected, the flow conditions required to achieve 71 kW were very different for hydrogen and helium ternary gases as noted in Fig. 2. The corresponding FFTs for the voltage and current signals are presented in Fig. 3 and 4, respectively. As can be seen, both FFTs are similar and the dominant Peak 1 frequency for the voltage fluctuation occurred around 20 kHz, whereas the dominant Peak 1 frequency for current was around 10 kHz. The calculated mean voltage (V), standard deviation (sd), amp factor (A), shape factor (Sh) for all the runs described in Table 1 are presented in Table 2. As shown here, the gun operates at a relatively high voltage compared to many commercial guns available in the market. This is due to the long arc that is established in this design. For all the runs described in Table 1, the Peak 1 and Peak 2 frequencies for the voltage signal occurred at 20 and 40 kHz, respectively. Typically, Peak 1 corresponds to the largest voltage fluctuations related to the connecting

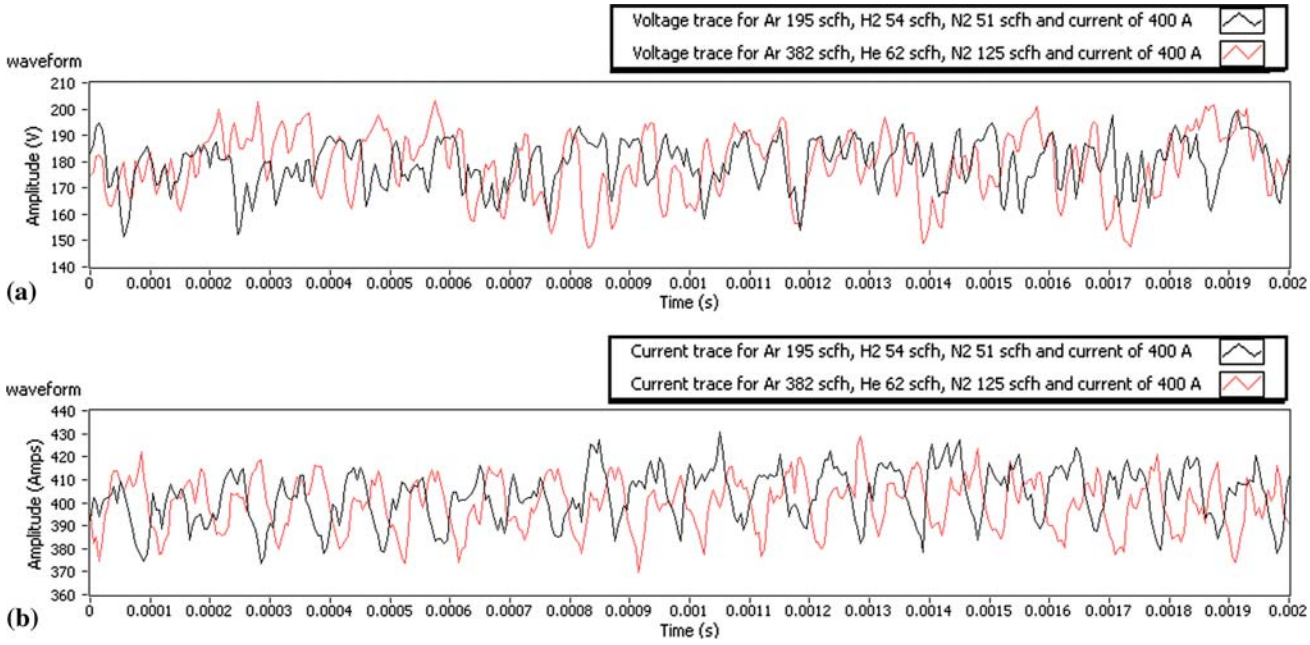

Fig. 2 Sample voltage-current traces using different ternary gases at 71 kW: (a) voltage and (b) current

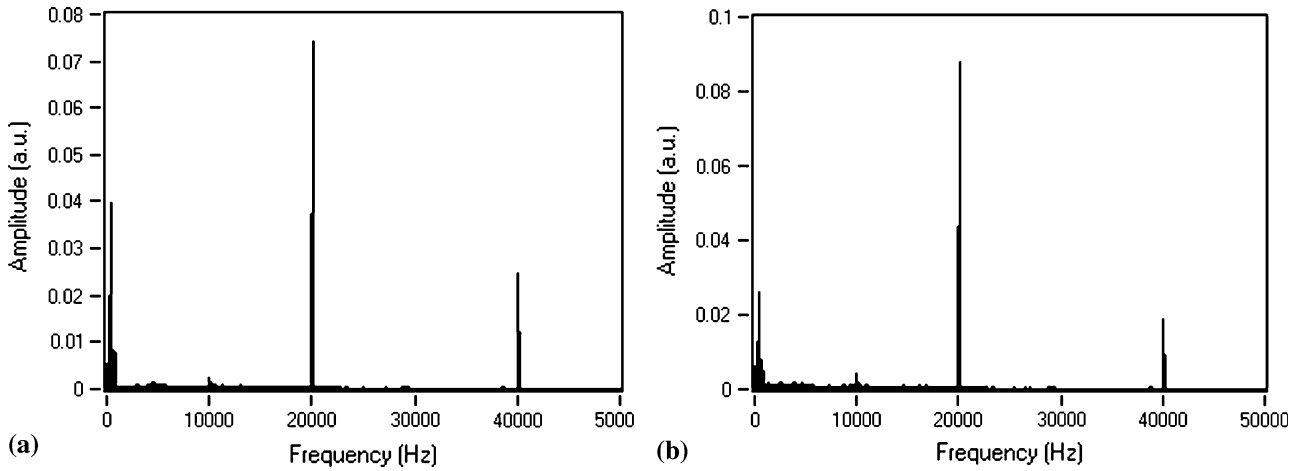

Fig. 3 The FFTs for voltage signals at two operating conditions presented in Fig. 2 (a, black; b, red)

arc column lengthening, Peak 2 corresponds to fluctuations due to turbulences or breakdown within the connecting column, and the third peak corresponds to acoustical signals which occur above 40 kHz (Ref 25). The Peak 1 and Peak 2 frequencies for the current signal also occurred at 10 and 20 kHz, respectively, even though the gun operated between 22 and 98 kW. The repeated occurrence of Peak 1 and Peak 2 (harmonics) frequencies at fixed values for all operating conditions suggests that these fluctuations emerge from a common source (the power source) rather than the arc. Incidentally, the switching frequency of the converter of our power supply (ESP-600C, ESAB Welding and Cutting Products, Florence, SC) is 10 kHz. This is possibly why the FFT of the current traces always showed the peak at 10 kHz and harmonics at 20 kHz. This needs to be verified independently by connecting a load bank to the power supply; however, this proved cost prohibitive at this time and would be attempted at a later date.

Figure 5 presents the standard deviation versus mean voltage plot. At 300 A as well as 400 A, the standard deviation increased with the mean voltage; however, the increase was very small. Particularly, for hydrogen ternary gas, the standard deviation varied from ~10.5 to 12.5 for a corresponding mean voltage variation of ~175 to 240. The change in standard deviation was bit stiffer for the case of helium ternary gas. The standard deviation is very different from many commercial guns studied earlier. For example, Nogues et al. (Ref 25) have presented the variation of standard deviation with respect to the mean

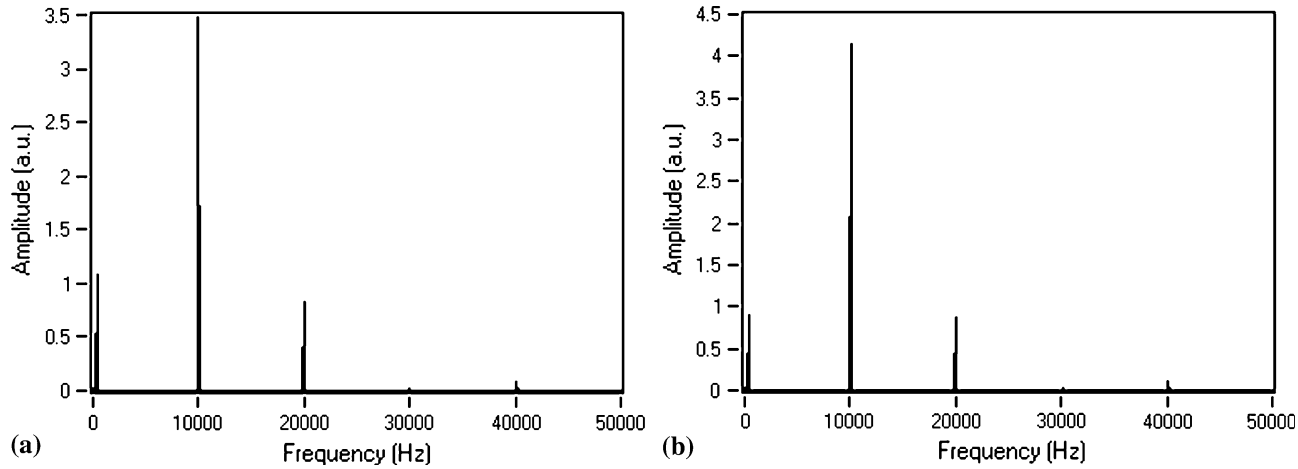

Fig. 4 The FFTs for current signals at two operating conditions presented in Fig. 2 (a, black; b, red)

Table 2 Voltage data

ID	Mean, $\bar{u}$, V	u_{sd}, V	*A*, %	*Sh*
100	175.0	11.05	6.317	2.125
101	177.74	10.84	6.098	2.144
102	181.83	10.39	5.714	2.020
103	239.28	12.15	5.077	1.852
104	244.82	12.75	5.207	2.083
105	244.69	12.65	5.169	2.082
200	105.6	6.09	5.767	2.111
201	116.28	7.12	6.129	2.385
202	124.71	8.18	6.558	2.459
203	153.51	11.21	7.303	2.146
204	168.2	12.69	7.549	2.090
205	179.80	13.33	7.413	2.029
300	181.71	10.71	5.894	1.839
301	183.44	10.61	5.783	1.723
302	183.09	10.37	5.663	1.705
303	244.94	12.85	5.246	3.153
304	244.74	13.04	5.330	3.039
305	245.74	12.89	5.247	2.719
400	109.12	7.00	6.414	2.234
401	118.63	8.08	6.818	2.224
402	126.58	9.06	7.157	2.212
403	158.8	11.56	7.279	2.071
404	169.38	11.56	6.824	2.047
405	182.14	11.34	6.225	2.004
500	190.79	11.06	5.799	3.604
501	189.91	11.12	5.855	3.774
502	185.39	11.25	6.068	3.695
503	248.08	9.62	3.877	1.632
504	246.11	9.82	3.990	1.669
505	246.98	9.58	3.878	1.630
600	108.68	10.34	5.799	3.604
601	123.11	9.26	5.204	2.152
602	132.7	9.78	7.521	2.158
603	162.89	8.73	7.370	2.233
604	175.17	8.31	5.359	2.197
605	187.47	8.45	4.743	2.186

voltage for the F4 and 3 MB plasma guns (Sulzer-Metco, Wohlen, Switzerland) at various operating conditions. Standard deviations up to ~30 were observed for a mean gun voltage of ~80 V.

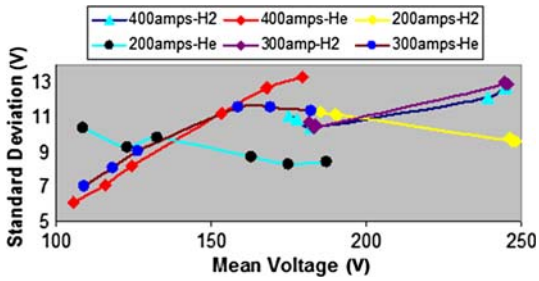

Fig. 5 Standard deviation vs. mean voltage

It is understood that the thinner the cold boundary layer (CBL) is, the lower are the voltage jumps and the shorter are the arc root lifetimes, leading to higher Peak 1 frequency. Experimental (Ref 11, 12) and numerical works (Ref 15) have shown that a stable behavior is observed when the time-evolution of the arc voltage exhibits a lower amplitude variation and a higher fluctuation frequency. In fact, the latter must be much higher than the characteristic time of particle acceleration and heating. Consequently, a better-quality coating (low porosity, low content of non-melted particles, and high deposition efficiency) is achieved. From the data presented in Table 2, it appears that in this design the CBL is very thin over a wide range of operating parameters, resulting in a very stable arc and lower voltage fluctuations. Over the parameter window studied here, the dominant Peak 1 frequency for all cases occurred near 20 kHz. As described above, the repeated occurrence of the Peak 1 at 20 kHz and Peak 2 at 40 kHz suggests that they emerge from a common source, i.e. the power supply. In other words, no significant fluctuations emerging from the arc were present due to the existence of a very thin cold boundary layer. However, the flow analysis in the plasma column does not support the above argument. Figure 6(a) presents the flow field in the plasma column of this design. The simulation was done using a volume

heating approach (Ref 18) in FLUENT (ANSYS, Canonsburg, PA) with gas flows as Ar-180 scfh, N_2-120 scfh, H_2-150 scfh, and current of 385 A. A sample flow field in the standard plasma column is also presented in Fig. 6(b). The parameters used in the second simulation

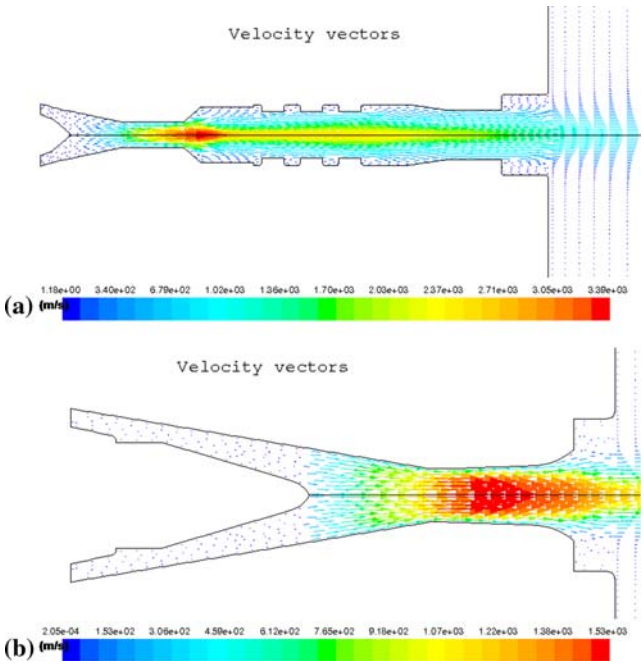

Fig. 6 Simulated flow patterns in the plasma column of (a) 100HE and (b) standard design

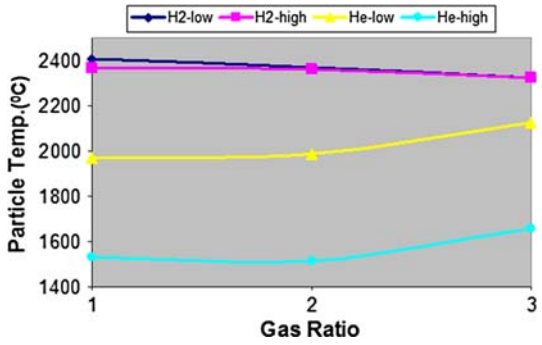

Fig. 7 Mean YSZ particle temperature at different gas ratios and 400 A

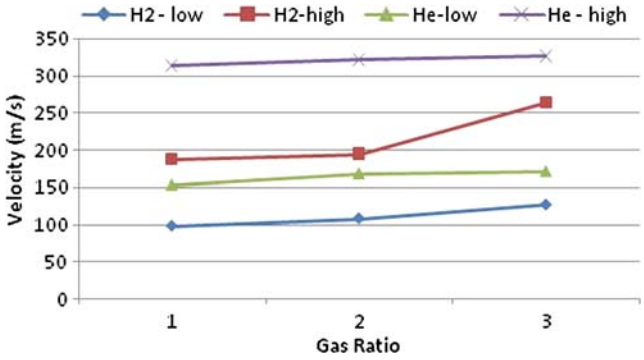

Fig. 8 Mean YSZ particle velocity at different gas ratios and 400 A

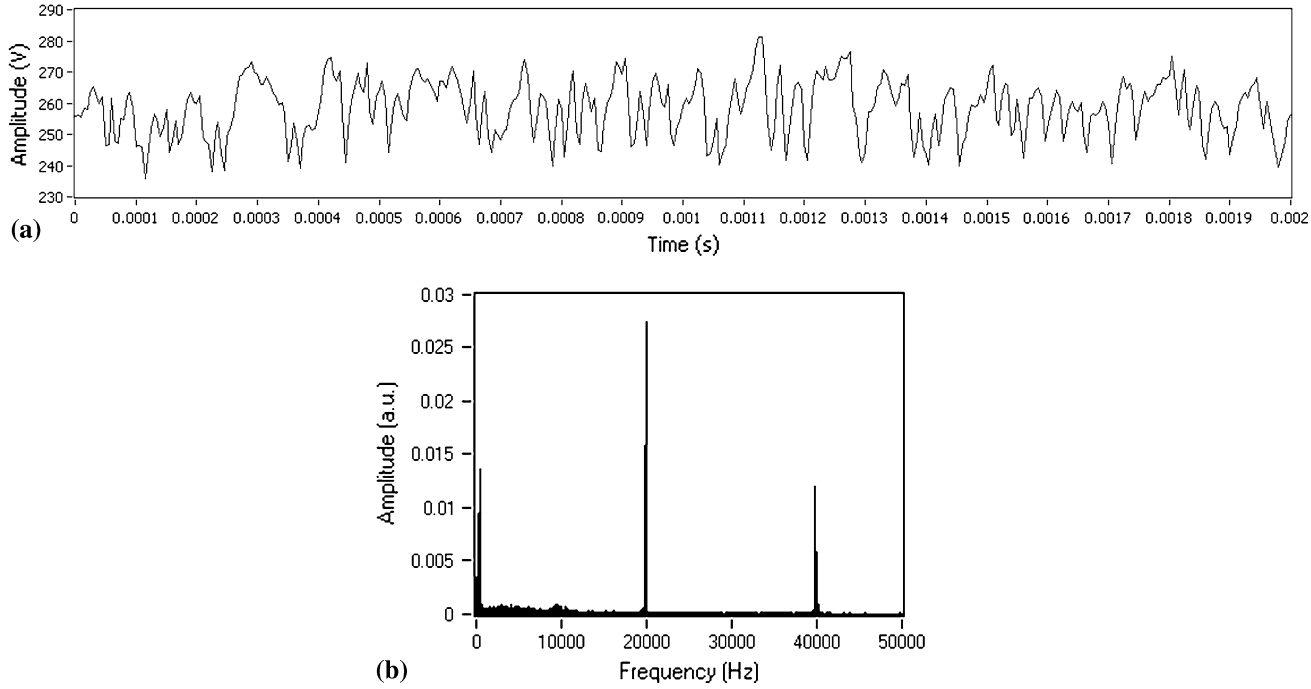

Fig. 9 (a) Voltage trace at 100 kW and (b) the corresponding FFT

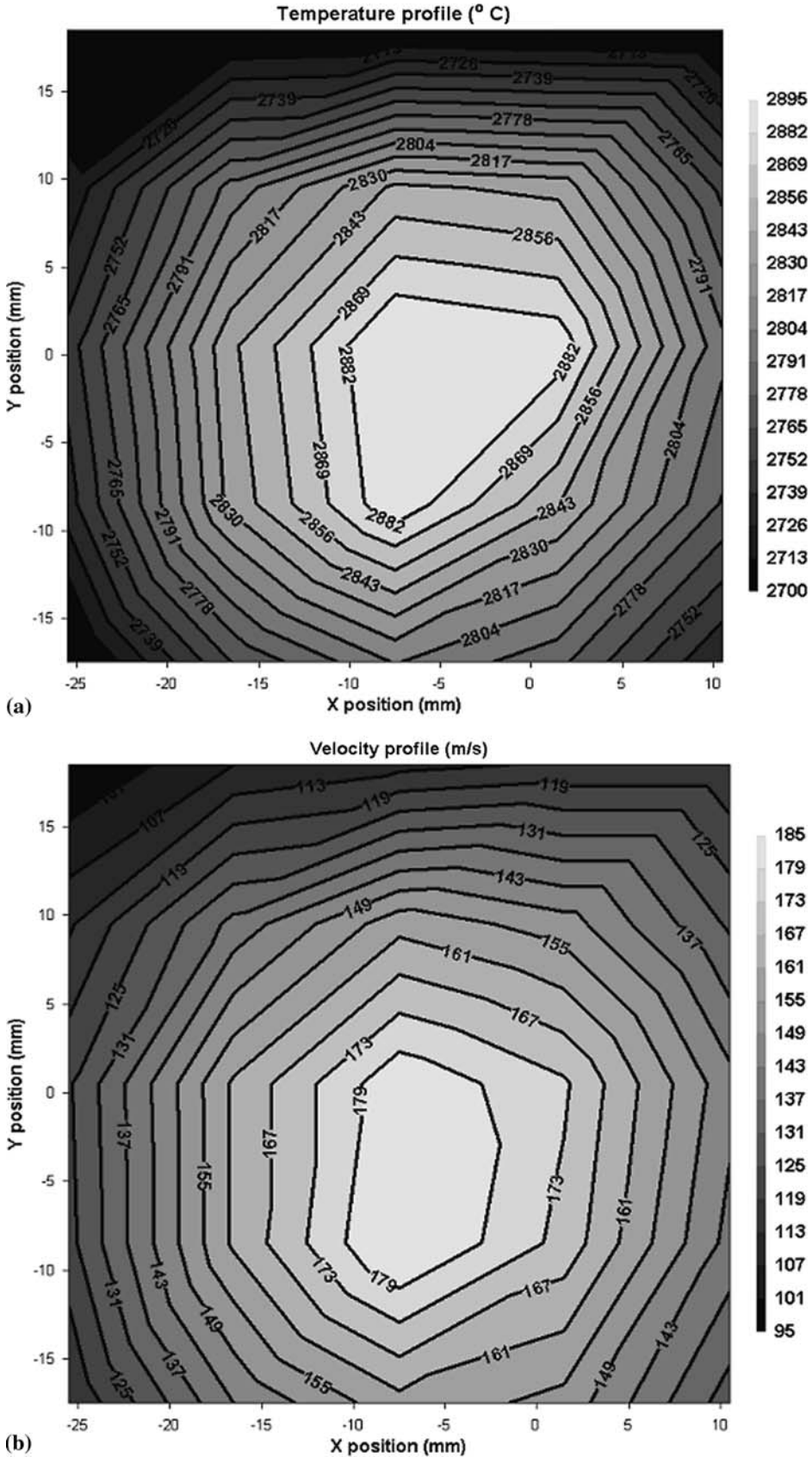

Fig. 10 (a) Plume cross section particle temperature and (b) plume cross section particle velocity

were Ar-71 scfh, He-4 scfh at 975 A. As expected, the gas velocities are much higher in the case of 100HE design due to high gas flow rates. Also, it is evident that the velocity gradient across the column is much stiffer in the case of 100HE compared to that of the standard configuration. It is understood that the use of high gas flow rates and diatomic plasma gases favor a thick cold gas boundary layer resulting in the so-called restrike mode (Ref 2). In this operation mode, the ''tongue'' that forms the current bridge between the main arc column and the anode wall is pushed forward by the gas flow in the outer layers of the main arc column until the cold boundary layer electrically breaks down. Thus, the arc voltage exhibits large fluctuations with a high mean value. Despite the stiffer velocity gradient, the use of diatomic secondary gas (N_2) and high mean voltage, the fluctuations were rather insignificant in this gun. To the best of our knowledge, such behavior has not been reported in any other single cathode gun operating in the voltage ranges considered here.

The influence of the ternary gas and the gas ratios on YSZ particle temperature and velocity (measured by DPV 2000 diagnostics system) are presented respectively in Fig. 7 and 8. As expected, H_2 ternary gas resulted in higher particle temperatures. It is to be noted that these are not the usual parameters for spraying YSZ. The particle temperatures for H_2 ternary gas were similar for both low and high flow conditions, whereas the particle velocities were significantly different. Normally, particle velocity and particle temperature go in opposite directions, as is the case for He. However, H_2 ternary gas and N_2 secondary gas enable one to achieve both higher temperature and velocity simultaneously. The mean voltage was more sensitive to the ternary gas type and flow conditions compared to the gas ratios. The density and the type of gas, the flow rates are expected to affect flow dynamics and consequently the mean velocity.

Although YSZ particles were used to study the influence of various gas ratios on the particle temperature and velocity, the typical spray parameters used for YSZ spraying are different than the ones discussed above. The typical spray parameters are Ar-180 scfh, N_2-120 scfh, H_2-150 scfh, current −385 A, and powder carrier gas-30 scfh. The powders were fed from two ports. The voltage trace at this operating condition and its FFT are presented in Fig. 9. The mean voltage and standard deviation were 258 and 9.74 V, respectively. Even when the gun was operating at around 100 kW, the voltage fluctuations were yet very small and the Peak 1 frequency occurred at 20 kHz (attributed to the power source). The plume cross section particle temperatures and velocities as determined by DPV 2000 are given in Fig. 10. As can be seen from Fig. 10(a), the temperature variation across the plume was small, whereas the velocity variation was quite significant (Fig. 10b).

To investigate the effect of anode and cathode separation, the length of the spacer ring between the constrictor and the anode was cut into half as shown in Fig. 11. The configuration in the left is the standard arrangement. To compensate for the decrease in the plasma column length, an extra ring was inserted after the anode as shown in the right. The corresponding voltage, current, and their FFT are presented in Fig. 12. This experiment was done under condition 501 (Table 1). The voltage characteristics now assume a restrike/takeover ($A = 16.3$, $Sh = 3.4$) mode with longer ramp up period followed by a sudden drop. The FFTs also show that the Peak 1 frequency for voltage occurs at a much lower value compared to the standard configuration. Also, in this case, the frequencies of the Peak 1 and Peak 2 changed with operating conditions unlike the case of standard hardware. Therefore, we believe that the peaks observed with the shortened spacer configuration were related to the arc behavior. This observation also reaffirms that in standard hardware, the steady occurrence of Peak 1 at 20 kHz and Peak 2 at 40 kHz emerged from the power source and they were apparent due to the absence of any significant fluctuations emerging from the arc. When the arc fluctuations became dominant due to the shortened distance between the anode and cathode, possibly the power supply signals were suppressed. However, the current peaks still occurred at fixed (10 and 20 kHz) frequencies even with shortened distance. They appear to be again associated with the power supply. A much broader study involving hardware configuration, arc behavior, and particle characteristics is underway and will be presented in future.

The performance of the gun ($Ar/N_2/H_2$: 200/100/120 slpm, 95 kW) over 16 h of continuous run is demonstrated through Fig. 13. As can be seen, the mean voltage, current, SS316 particle velocity and temperature (measured by SprayWatch 2i) remained fairly stable. Although the 16 h run is not long enough to demonstrate the long-term

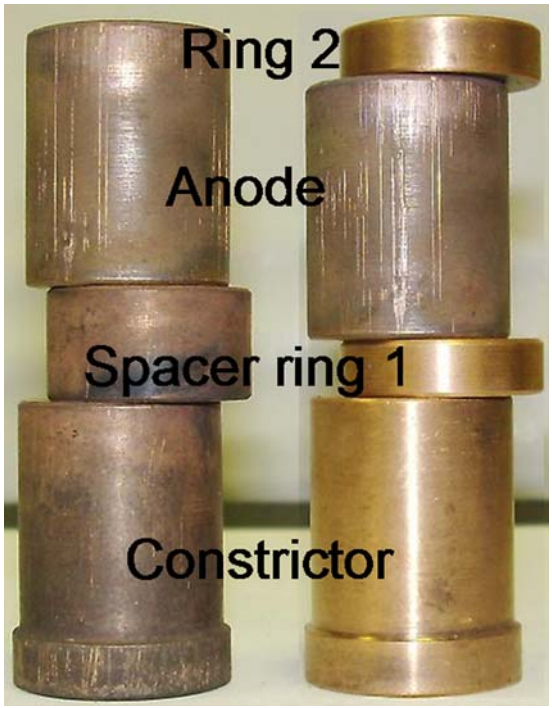

Fig. 11 Spacer rings used to change distance between cathode and anode

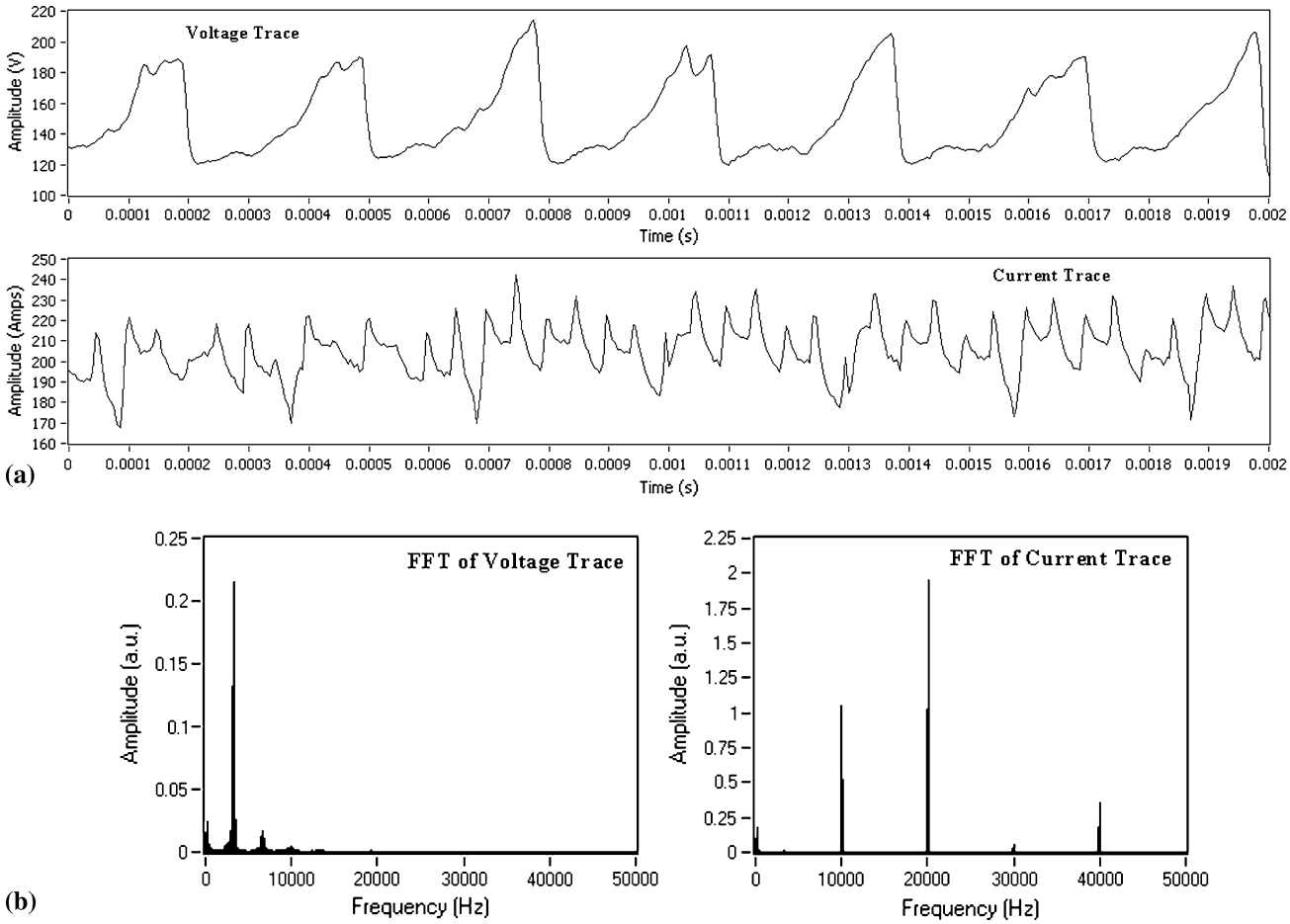

Fig. 12 (a) Voltage and current traces at reduced distance between the cathode and anode; (b) the corresponding FFTs of voltage and current traces

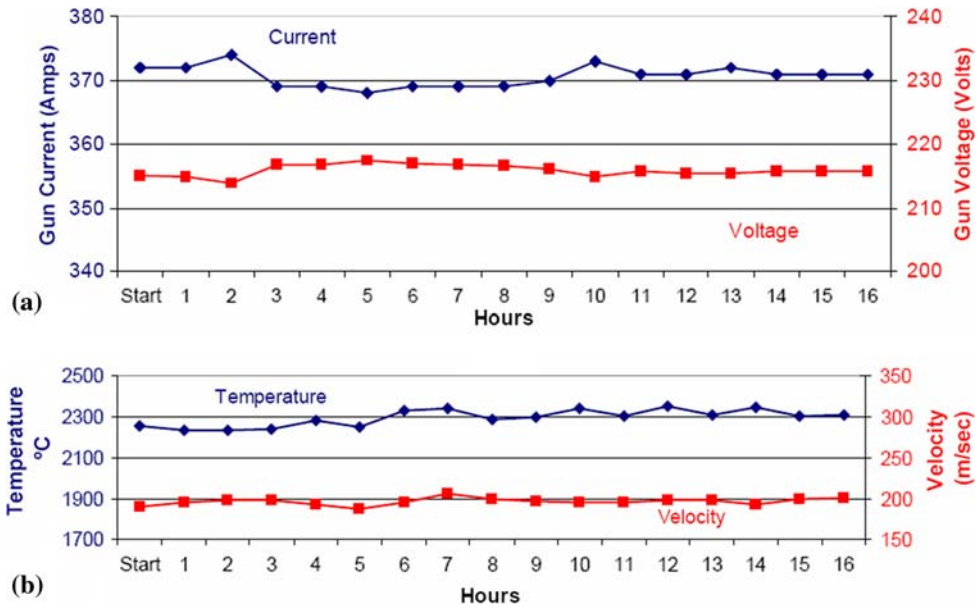

Fig. 13 (a) The 16 h mean voltage and current traces; (b) corresponding SS316 particle temperature and velocity. (Ar-240, $N_2 = 100$, $h_2 = 60$, all values in scfh)

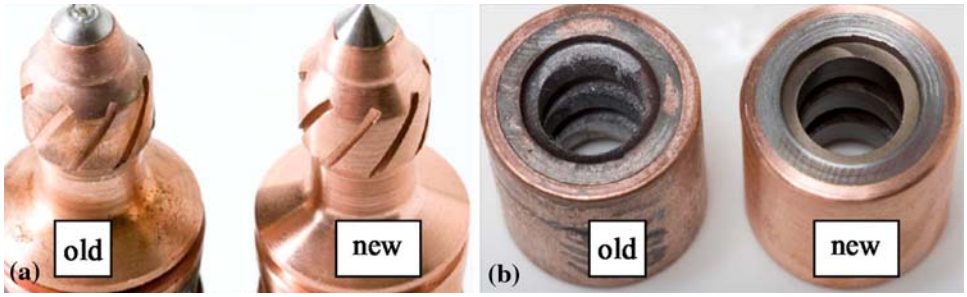

Fig. 14 (a) Cathode after 200 h run and (b) anode after 1500 h run

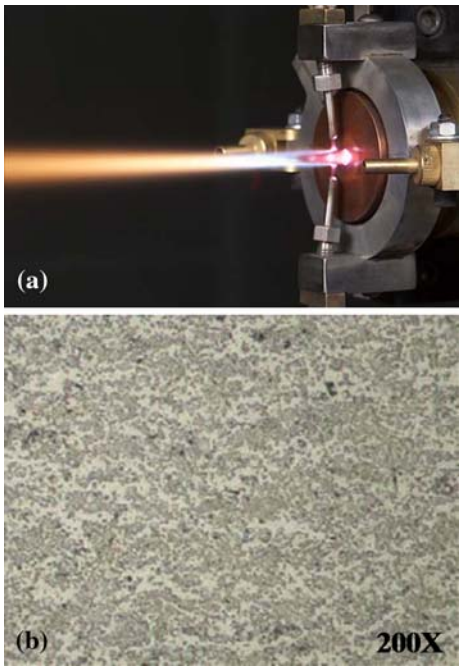

Fig. 15 (a) High-velocity mode operation and (b) WC-12%Co coating

stability, but Leblanc and Moreau (Ref 12) have shown a 5-6% drop in gun mean voltage within the first 15 h of operation in F4 gun. That kind of drop was not observed in the 100HE gun. Further, the typical life of an anode in a standard gun (SG100) is about 300 h. The typical life of the anode in the 100HE gun is more than 1000 h. An anode functioning after 1500 h (Fig. 14) does demonstrate the effect of arc stability on the component life of this system.

Figure 15(a) demonstrates the plasma jet reaching the characteristics of an HVOF jet. The operating conditions were Ar-142 L/min, N_2-56.6 L/min, H_2-23.6 L/min and 90 kW. Particle velocities up to 527 m/s and temperature ~1882 ± 33 °C were recorded by SprayWatch 2i, using ~45 μm WC-12%Co powders. The resulting coating microstructure is presented in Fig. 15(b), which has the appearance of a HVOF coating. The deposition efficiency was estimated to be around 80% with average hardness value of 1141 Hv. This further demonstrates the uniqueness and range of operational window possible with this design.

4. Conclusions

A novel single cathode plasma column design is investigated in this study. The electrical signals and their analysis demonstrated a very stable arc behavior over a wide operational window. For most cases, the operational mode appears to be a mix of the steady and takeover modes. Despite high mean voltage, the standard deviations were much smaller than the deviations reported in other commercial guns. Although diatomic gases were used and high gas velocities existed in the plasma column, the so-called ''restriking'' did not appear to occur in this system. This is contrary to many observations reported in other commercial systems. However, when the distance between the cathode and anode was reduced, the arc did exhibit some restriking behavior. The steady arc behavior results in wide operational window reaching the HVOF characteristics as well as long component life.

Acknowledgments

Financial support from the US Navy under contract no. N00244-07-P-0553 is gratefully acknowledged. The authors are thankful to Bill Barker and Progressive Technologies Inc., for this collaboration.

References

1. J. Hlina and V. Nénicka, Identification of Local Oscillations in a Plasma Jet, *Prog. Plasma Process. Mater.,* 1999, p 333-337
2. Z. Duan and J. Heberlein, Arc Instabilities in a Plasma Spray Torch, *J. Therm. Spray Technol.*, 2002, **11**, p 44-51
3. H.P. Li, J. Heberlein, and E. Pfender, Three-Dimensional Nonequilibrium Effects in a High-Intensity Blown Arc, *IEEE Trans. Plasma Sci.*, 2005, **33**(2), p 402-403
4. J.P. Trelles and J. Heberlein, Simulation Results of Arc Behavior in Different Plasma Spray Torches, *J. Therm. Spray Technol.*, 2006, **15**(4), p 563-569
5. J.P. Trelles, E. Pfender, and J. Heberlein, Multi Scale Element Modeling of Arc Dynamics in a D.C. Plasma Torch, *Plasma. Chem. Plasma Process.*, 2006, **26**, p 557-575

6. H.P. Li and E. Pfender, Three Dimensional 3D Simulation of a DC Transferred Arc Plasma Modeling of the Plasma Spray Process, *J. Therm. Spray Technol.*, 2007, **16**(2), p 245-260
7. J.P. Trelles, J. Heberlein, and E. Pfender, Non-Equilibrium Modelling of Arc Plasma Torches, *J. Phys. D: Appl. Phys.*, 2007, **40**, p 5932-5937
8. J.P. Trelles, E. Pfender, and J. Heberlein, Thermal Nonequilibrium Simulation of an Arc Plasma Jet, *IEEE Trans. Plasma Sci.*, 2008, **36**(4), p 1026-1027
9. C. Chazelas, J.F. Coudert, and P. Fauchais, Arc Root Behavior in Plasma Spray Torch, *IEEE Trans. Plasma Sci.*, 2005, **33**(2), p 414-420
10. J. Dorier, M. Gindrat, C. Hollenstein, A. Salito, M. Loch, and G. Barbezat, Time-Resolved Imaging of Anodic Arc Root Behavior During Fluctuations of a DC Plasma Spraying Torch, *IEEE Trans. Plasma Sci.*, 2001, **29**(3), p 494-501
11. J.F. Bisson, B. Gautier, and C. Moreau, Effect of Plasma Fluctuations on In-flight Particle, *J. Therm. Spray Technol.*, 2003, **12**, p 38-43
12. L. Leblanc and C. Moreau, The Long-Term Stability of Plasma Spraying, *J. Therm. Spray. Technol.*, 2002, **11**(3), p 380-386
13. S. Janisson, A. Vardelle, J.F. Coudert, E. Meillot, B. Pateyron, and P. Fauchais, Plasma Spraying Using Ar-He-H_2 Gas Mixtures, *J. Therm. Spray. Technol.*, 1999, **8**(4), p 545-552
14. R. Hartmann and J. Heberlein, Quantitative Investigations on Arc-Anode Attachments in Transferred Arcs, *J. Phys. D: Appl. Phys.*, 2001, **34**(19), p 2972-2978
15. E. Moreau, C. Chazelas, G. Mariaux, and A. Vardelle, Modeling the Restrike Mode Operation of a DC Plasma Spray Torch, *J. Therm. Spray. Technol.*, 2006, **15**(4), p 524-530
16. P. Fauchais, Understanding Plasma Spraying, *J. Phys. D: Appl. Phys.*, 2004, **37**, p R86-R108
17. X. Tu, J.H. Yan, B.G. Chéron, and K.F. Cen, Fluctuations of DC Atmospheric Double Arc Argon Plasma Jet, *Vacuum*, 2008, **82**, p 468-475
18. D. Hawley, A. Refke, and K.D. Landis, Plasma Plume Condition Forming of Cascaded Type Plasma Guns, *Thermal Spray: Thermal Spray Connects*, E. Lugscheider, Ed., May 2-4, 2005 (Basel, Switzerland), ASM International, 2005, p 465-469
19. T. Sugimoto and M. Horenstein, Design of a Circular Cascaded Arc Torch Array for Plasma Spray, *J. Therm. Spray. Technol.*, 2003, **12**(4), p 536-541
20. R. Molz, R. McCullough, D. Hawley, and F. Muggli, Improvement of Plasma Gun Performance Using Comprehensive Fluid Element Modeling II, *J. Therm. Spray. Technol.*, 2007, **16**(5-6), p 684-689
21. L.B. Delcea, Anode Electrode for Plasmatron Structure, U.S. Patent 6,114,649, 5 Sept 2000
22. T.F. Bernecki, K.J. Varley, W.P. Rusch, J. Wlodarczyk, and J.F. Klein, Plasma Gun with Adjustable Cathode, U.S. Patent 4,780,591, 25 Oct 1988
23. L.P. Dorfman, S. Sampath, M.J. Scheithauer, and J.E. Vanderpool, Vortex Arc Generator and Method of Controlling the Length of the Arc, U.S. Patent 5,374,802, 20 Dec 1994
24. M. Vysohlid and J. Heberlein, Investigation of Arc Voltage Fluctuations in a Plasma Torch SG-100 Operated with Ar/H_2, *Proceedings of the International Thermal Spray Conference*, May 10-12, 2004 (Osaka, Japan), ASM International, 2004, p 998-1003
25. E. Nogués, P. Fauchais, M. Vardelle, and P. Granger, Relation Between the Arc-Root Fluctuations, the Cold Boundary Layer Thickness and the Particle Thermal Treatment, *J. Therm. Spray Technol.*, 2007, **16**(5-6), p 919-926